

An RXTE Observation of the Seyfert 1 Galaxy MCG–6-30-15 : X-ray Reflection and the Iron Abundance

J.C. Lee,¹ A.C. Fabian¹, C.S. Reynolds,² K. Iwasawa,¹ and W.N. Brandt³

¹ *Institute of Astronomy; Madingley Road; Cambridge CB3 0HA*

² *JILA; Campus Box 440; University of Colorado; Boulder, 80309-0440 USA*

³ *Department of Astronomy and Astrophysics; The Pennsylvania State University; 525 Davey Lab; University Park, PA 16802 USA*

11 June 2021

ABSTRACT

We report on a 50 ks observation of the bright Seyfert 1 galaxy MCG–6-30-15 with the *Rossi X-ray Timing Explorer*. The data clearly show the broad fluorescent iron line (equivalent width ~ 250 eV), and the Compton reflection continuum at higher energies. A comparison of the iron line and the reflection continuum has enabled us to constrain reflective fraction and the elemental abundances in the accretion disk. Temporal studies provide evidence that spectral variability is due to changes in both the amount of reflection seen and the properties of the primary X-ray source itself.

Key words: galaxies:active - X-ray:galaxies - galaxies:individual:MCG–6-30-15 - accretion,accretion discs

1 INTRODUCTION

The current paradigm for active galactic nuclei (AGN) is a central engine consisting of an accretion disk surrounding a supermassive black hole (e.g., see review by Rees 1984). The main source of power is the release of gravitational potential energy as matter falls towards the central black hole. Much of this energy is released in the form of X-rays, some fraction of which are reprocessed by matter in the AGN (Guilbert & Rees 1988; Lightman & White 1988).

Careful study of the X-ray reprocessing mechanisms can give much information about the immediate environment of the accreting black hole. These effects of reprocessing can often be observed in the form of emission and absorption features in the X-ray spectra of AGNs. In Seyfert 1 nuclei, approximately half of the X-rays are ‘reflected’ off the inner regions of the accretion disk. Since it is superposed on the direct (power-law) primary X-ray emission, the principle observables of this reflection are a fluorescent iron $K\alpha$ line, and a Compton backscattered continuum which hardens the observed spectrum above ~ 10 keV (see eg. George & Fabian 1991). The iron line together with the reflection component are important diagnostics for the geometry and physics of the X-ray continuum source. The strength of the emission line relative to the reflection continuum depends largely on the abundance of iron relative to hydrogen in the disk, as well as the normalization of the reflection spectrum relative to the direct spectrum. (There is also a dependence on the relative oxygen abundance, Reynolds et al. 1995.) The relative normalization of the reflection spectrum probably depends primarily on the geometry (i.e., the solid angle subtended by the reflecting parts of the disk as seen by the X-ray source). However, it can also be affected by strong light bending effects (e.g., Martocchia & Matt 1996) or special-relativistic beaming effects (e.g. Reynolds & Fabian 1997). Disentangling the abundance

from the absolute normalization of the reflection component is an important first step in constraining these effects and hence the construction of physical models for AGN central regions.

MCG–6-30-15 is a Seyfert 1 galaxy that is both bright and nearby ($z=0.008$). Since its identification, MCG–6-30-15 has been intensively studied by every major X-ray observatory. An extended *EXOSAT* observation provided the first evidence for fluorescent iron line emission (Nandra et al. 1989) which was attributed to X-ray reflection. Confirmation of these iron features by *Ginga* as well as the discovery of the associated Compton reflected continuum supported the reflection picture (Nandra, Pounds & Stewart 1990; Pounds et al. 1990; Matsuoka et al. 1990). ASCA data showed the iron line to be broad, skewed, and variable (eg. Tanaka et al 1995; Iwasawa et al. 1997).

In this paper, we present the first data from the *Rossi X-ray Timing Explorer* (*RXTE*) for MCG–6-30-15. Our observation shows clear evidence for a redshifted broad iron line at ~ 6.1 keV and the reflection continuum above 10 keV. Due to the larger effective area and longer exposure of the *RXTE* observation as compared with *Ginga*, we can study the reflection continuum in detail for the first time. We present preliminary constraints on the abundances of iron and reflective fraction, and investigate the relationship between spectral changes and the reflection component during the different phases of our data. Section 2 will detail the data analysis procedure followed by spectral fitting results in Section 3. We present a study of temporal variations on spectral components with particular emphasis on the reflection component in Section 4. This will follow with a discussion of results and future work in Section 5.

2 OBSERVATIONS

MCG–6-30-15 was observed by the *RXTE* for 50 ks over the period from 1996 September 15 to 1996 September 25 by both the Proportional Counter Array (PCA) and High-Energy X-ray Timing Experiment (HEXTE) instruments. We concentrate on results from the PCA in this paper.

2.1 Proportional Counter Array

The *RXTE* PCA consists of 5 Xenon Proportional Counter Units (PCUs) sensitive to X-ray energies between 2–60 keV with ~ 18 per cent energy resolution at 6 keV. The total collecting area is 6500 cm² (~ 3900 cm² for 3 PCUs) with a 1° FWHM field of view. The HEXTE instrument is coaligned with the PCA and covers an energy range between 20–200 keV; these results will be discussed in a later paper.

2.2 Data Analysis

We extract PCA light curves and spectra from only the top Xenon layer using the standard *Ftools* 4.0 software developed specifically for *RXTE*. This was done to improve the signal-to-noise since the top layer detects ~ 90 per cent of the cosmic photons and ~ 50 per cent of the internal instrumental background. At the expense of slightly blurring the spectral resolution, we also combine data from three of the five PCUs in order to improve signal-to-noise. Data from the remaining PCUs (PCU 3 and 4) were excluded due to the fact that these instruments periodically suffer discharge and are hence sometimes turned off.

Good time intervals were selected to exclude any earth or South Atlantic Anomaly (SAA) passage occultations, and to ensure stable pointing. We also require that data from only PCUs 0, 1, and 2 were used.

We generate our background data using *PCABACKEST* v1.5 in order to estimate the internal background caused by interactions between the radiation / particles and the detector / spacecraft at the time of observation. This is done by matching the conditions of observations with those in various model files. The model files that we chose were constructed using the VLE rate (one of the rates in PCA Standard 2 science array data that is defined to be the rate of events which saturate the analog electronics) as the tracer of the particle background. Other models such as the Q6 (short for Standard 2 telemetry rate) background model exist and is based on the rate of events which trigger exactly six of the eight signal channels. Both models are believed to be a measure of the instantaneous particle flux (Keith Jahoda, 1997 private communication). While the choice between these two types of models is based largely on value judgements (neither is perfect at present), we find that the VLE background models provide a better estimate of the background in a test using Earth occultation data from our observations.

There was no need to apply a deadtime correction for our PCA data since deadtime exceeds 1 per cent only when the count rate per PCU is greater than 1000 cts s⁻¹. The 3 PCU count rate for MCG–6-30-15 is $\sim 5 - 30$ cts s⁻¹ for the background subtracted source (Fig. 1), and $\sim 50 - 80$ cts s⁻¹ prior to background subtraction (Fig. 2).

The PCA response matrix for this data set was created by adding together the individual response matrices for PCUs 0, 1, and 2. These individual matrices were provided by the *RXTE* Guest Observer Facility (GOF) at Goddard Space Flight Center and are representative of the most up-to-date PCA calibration.

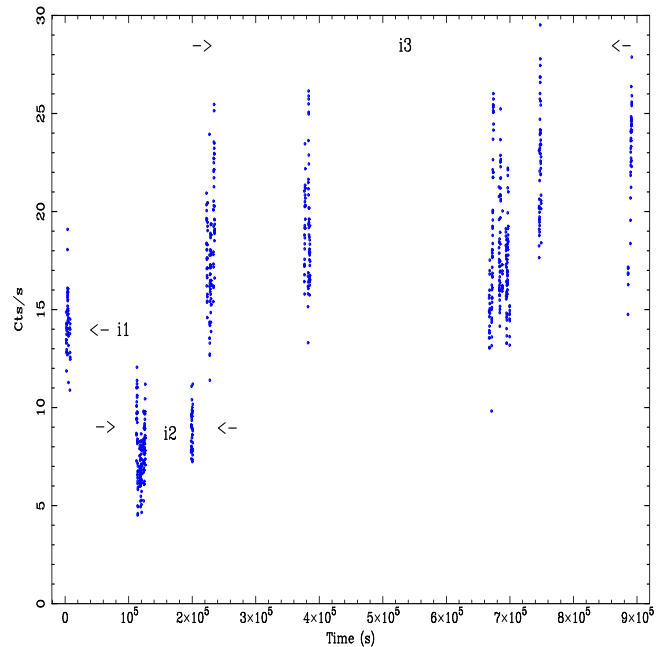


Figure 1. Background-subtracted light curve of MCG–6-30-15 for observations with 3 PCUs in the 2–60 keV band. The epoch of the start and end time is respectively 1996 September 15, 15:24:17 (UT) and 1996 September 25, 23:08:13 (UT). Time intervals for the three spectral phases of light curve correspond roughly to time intervals $0 - 3 \times 10^3$, $1 \times 10^5 - 2 \times 10^5$, and $2 \times 10^5 - 9 \times 10^5$ seconds.

Figure 1 shows the background subtracted PCA light curve of our observation over the whole PCA energy band (2–60 keV). Significant variability can be seen during the ~ 900 ks over which our observations were made.

3 SPECTRAL FITTING

We fit the data in two ways in order to investigate the known features of reflection and fluorescent iron emission. A detector Xe feature previously detected at ~ 4 keV leads us to assume that the possibility of inadequate calibration below this energy may still exist; uncertainties in calibration certainly still exist below 2 keV. However, for fairly faint sources such as AGN, background subtraction is the main source of concern in any *RXTE* analysis. We present in Fig. 2 light curves showing both the source prior to background subtraction as well as the background light curve to give an indication of the overall background contribution to our observation. Similarly, a plot of source and background spectra show that background effects become significant past 20 keV (Fig. 3). The standard background subtraction methods described in Section 2.2 should adequately account for the background up until this energy. We therefore concentrate on the energy range between 4 and 20 keV for our fits. As added checks for the quality of our reduction, background subtraction and PCA calibrations, we extract spectra from our 400 s observations of Earth occulted data ($ELV \leq 0$), and a 1.9 ks exposure of archived Crab data from the same gain epoch (epoch 3) as our observations. We find for the occultation data that the normalized flux per keV is essentially zero for the background subtracted source in the energy range of interest. A power law fit to the spectrum of the Crab using the most recent response matrices and background models gives residuals less than 1 per cent for the

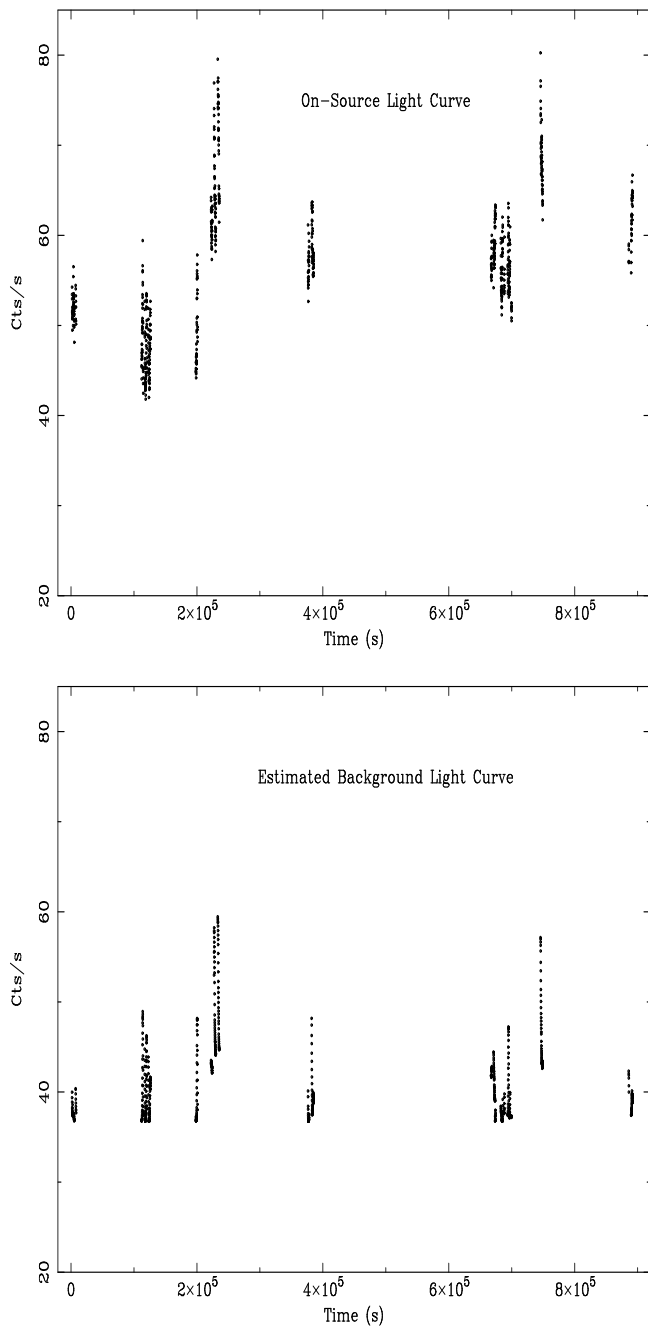


Figure 2. Source and background light curve of MCG–6-30-15 for observations with 3 PCUs in the 2-60 keV band. The epoch of the start and end time is respectively 1996 September 15, 15:24:17 (UT) and 1996 September 25, 23:08:13 (UT).

energies of interest. These checks give us extra confidence in our background subtraction and calibration files. We add a 1 per cent systematic error to account for problems with calibration.

We also note that restricting our analysis to data above 4 keV removes the need to model the photoelectric absorption due to Galactic ISM material, or the warm absorber that is known to be present in this object. Both of these spectral features are only important below ~ 2 keV (Reynolds et al. 1995; Otani et al. 1996).

In order to investigate the effects of spectral changes on the photon index and intensity of the Fe line, we also explore the behavior of the light curve in its 3 spectral states (Fig. 1) in Section 4.

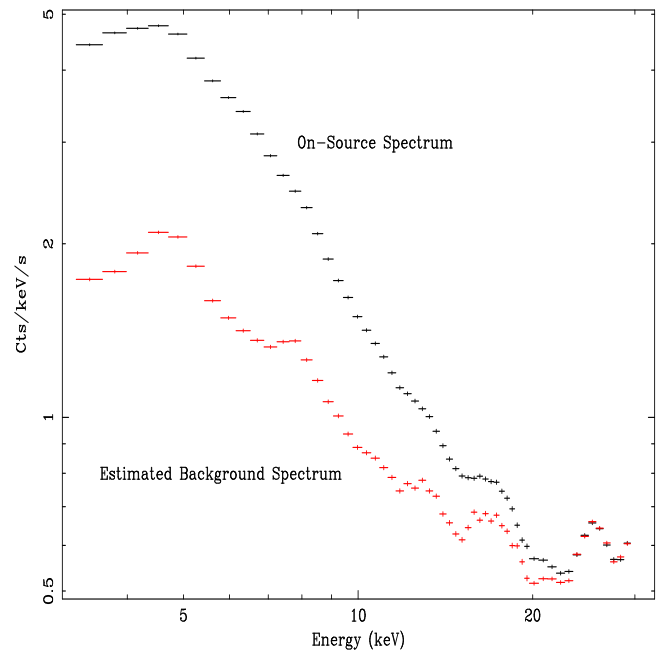


Figure 3. Plot of total on-source (i.e. source+background) and background spectra in the energy range $3 \text{ keV} < E < 30 \text{ keV}$ show that background effects are significant only past 20 keV.

3.1 Simple Power Law Fits

A naive fit using a simple power law shows the presence of a redshifted broad iron line at ~ 6.1 keV and strong reflection continuum above 10 keV (Fig. 4). Previous ASCA results have resolved the presence of a broad iron line in MCG–6-30-15 (Fabian et al. 1994a; Tanaka et al. 1995) and reflection was reported with GINGA for a number of Seyfert 1 AGNs (Pounds et al. 1990; Matsuoka et al 1990; Nandra & Pounds 1994). Due to the improved signal-to-noise (as compared with *Ginga*) and higher energy coverage (as compared with ASCA) afforded by *RXTE*, we are able to report here on one of the first results where the simultaneous strong presence of both features is evident.

3.2 Fits using power law with reflection and line emission

The simple power law fit having proven insufficient, we investigate a multiple component model consisting of a power law, reflection continuum and gaussian component (to model the iron emission line). We fit the underlying continuum using the model PEXRAV which is a power law with an exponential cut off at high energies reflected by an optically thick slab of neutral material (Magdziarz and Zdziarski 1995). We fix the inclination angle of the reflector at 30° so as to agree with the disk inclination one obtains when fitting accretion disk models to the iron line profile as seen by ASCA (Tanaka et al. 1995). For completeness, we consider the effect of the $2^\circ - 3^\circ$ uncertainty associated with ASCA's determination of the iron line inclination angle. This should be a negligible effect since the reflected component is insensitive to this parameter. We confirm this when we compare contour plots of abundance versus reflective fraction for inclination angles of $30 \pm 5^\circ$ and find them to be similar. The reflective fraction is defined such that its value equal to unity implies that the reflecting matter subtends half of the sky ($\Omega = 2\pi$).

First, we shall address the formal detectability of the iron line

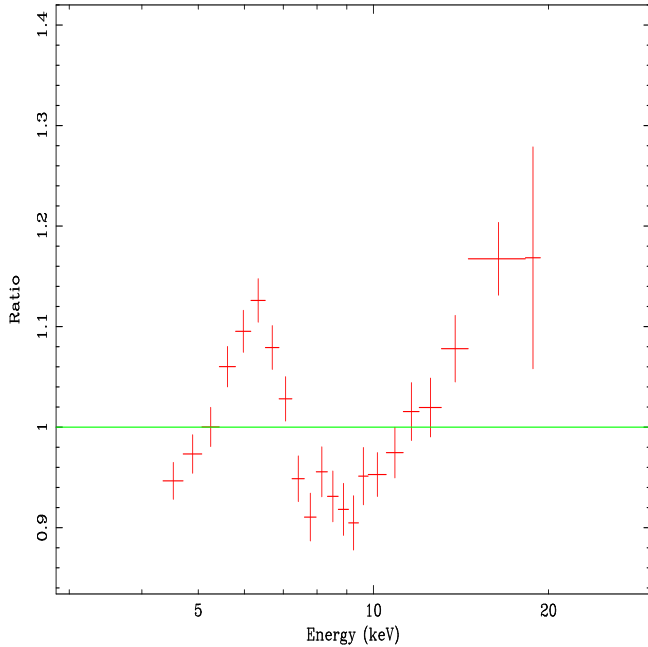


Figure 4. Ratio of data to continuum when a simple power law is used to fit MCG–6-30-15 spectra. There is clear evidence for a redshifted broad iron line at ~ 6.1 keV and reflection continuum above 10 keV. This is consistent with previous GINGA findings for the existence of a reflection component in many Seyfert 1 AGNs.

and the resolution of its width. Fitting the above continuum model, and then adding a narrow iron line (with energy as a free parameter) leads to an improvement in the goodness of fit of $\Delta\chi^2 = 27$ for two extra parameters, more than 99 per cent significant according to the *F-test* for 35 degrees of freedom. Allowing the line width to be a free parameter leads to a further improvement of $\Delta\chi^2 = 7$ for one additional parameter, with the best fit line width $\sigma = 0.55^{+0.29}_{-0.22}$, more than 99 per cent significant according to the *F-test*. We conclude that the line is both detected and resolved. Motivated by the best fit line width, and previous *ASCA* results, we shall fix $\sigma = 0.4$ keV for our future spectral fits.

We find that the best fit is given by a redshifted broad iron line having an energy of $6.15^{+0.13}_{-0.12}$ keV and equivalent width $\text{EW} = 223^{+41}_{-57}$ eV. With the lighter elemental abundances (eg. oxygen) set equal to that of iron, we find abundance measurements to be $0.77^{+4.33}_{-0.25}$ solar abundances with an associated reflective fraction of $1.43^{+1.23}_{-0.51}$ and spectral index $\Gamma = 2.25^{+0.22}_{-0.09}$ at the 90 per cent confidence level. At 68 per cent confidence, abundance and reflective fraction are respectively $0.77^{+0.39}_{-0.18}$ solar abundances and $1.44^{+0.57}_{-0.36}$. The overall χ^2/ν is 0.92 for 35 degrees of freedom. Figure 5 demonstrates that this model describes the 4–20 keV data well (i.e., there are no systematic deviations of the data from the model). As expected, there is a strong coupling between the fit parameters. In particular, the power-law index, the elemental abundances and the reflective fraction are strongly coupled. Figure 6 shows the confidence contours for abundance and reflective fraction as expected from a corona+disk model. We note that there are a number of scenarios in which the reflected spectrum can be enhanced (reflective fraction > 1). These can include effects due to geometry (ie. where the direct X-ray flares are partially obscured), motion of the source (e.g. Reynolds & Fabian 1997), or gravity (light-bending effects that will beam/focus more of the emission down towards the disk

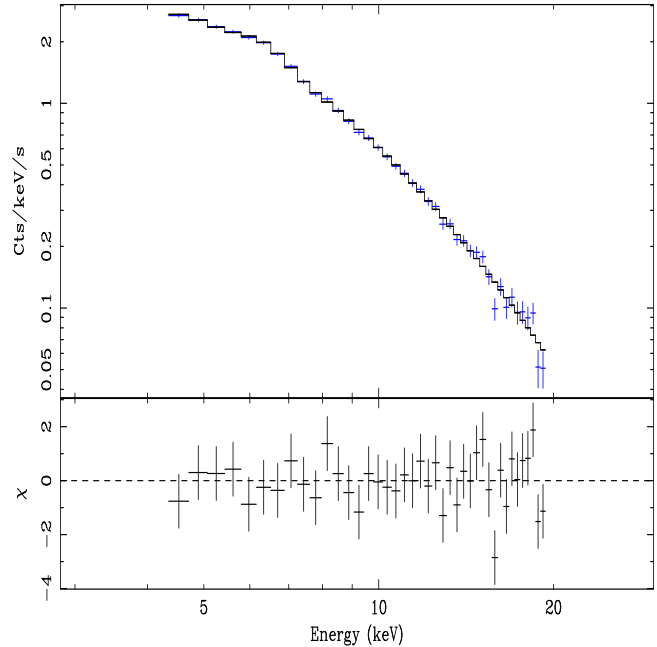


Figure 5. A more sophisticated multiple component model fit consisting of a gaussian component to represent the iron $K\alpha$ emission, and a power law reflection component to model the primary and reflected continuum is needed to fit the data well.

; Martocchia & Matt 1996) in addition to a number of other possibilities.

In a fit where we further assume that the primary X-ray source is above the accretion disk subtending an angle of 2π sr (ie $\frac{\Omega}{2\pi} = 1$), we find the best fit to be: $\Gamma = 2.15^{+0.11}_{-0.11}$ (this value is slightly steeper than previous *ASCA* and *Ginga* measurements) with the power law flux at 1 keV, $A = (2.53 \pm 0.36) \times 10^{-2}$ ph cm $^{-2}$ s $^{-1}$, the redshifted line energy is 6.13 ± 0.16 keV with intensity of the iron line $I = 1.47^{+0.18}_{-0.47} \times 10^{-4}$ ph cm $^{-2}$ s $^{-1}$ and $\text{EW} = 257^{+32}_{-81}$ eV. All abundances again set equal to that of iron, we find values for abundances to be $0.80^{+0.46}_{-0.3}$ and $0.80^{+0.16}_{-0.19}$ solar abundances for 90 and 68 per cent confidence respectively. χ^2/ν is 1.00 for 36 degrees of freedom. It should be noted that even though we set the lighter elemental abundances equal to that of iron, we expect that iron is primary in determining the fitted abundances since the reflection continuum is only important at energies past 10 keV where iron absorption dominates. The significance of iron in affecting abundance values is confirmed when the lower elemental abundances are decoupled from that of iron abundances.

The relatively steep intrinsic photon index of MCG–6-30-15 is worth noting. Previous studies have found a strong anticorrelation between Γ and the full width at half-maximum (FWHM) of the $H\beta$ emission line for Seyfert 1 type galaxies in both the soft *ROSAT* band (eg. Boller, Brandt & Fink 1996) and *ASCA* hard band (eg. Brandt, Mathur, & Elvis 1997). A recent multiwavelength study of MCG–6-30-15 by Reynolds, *et al.* 1997 find FWHM of $H\beta$ in the optical band to be 2400 ± 200 km/s for this object. Given the steep intrinsic photon index that we find for MCG–6-30-15, this implies that MCG–6-30-15 could possibly be categorized as a narrow-line Seyfert 1 galaxy.

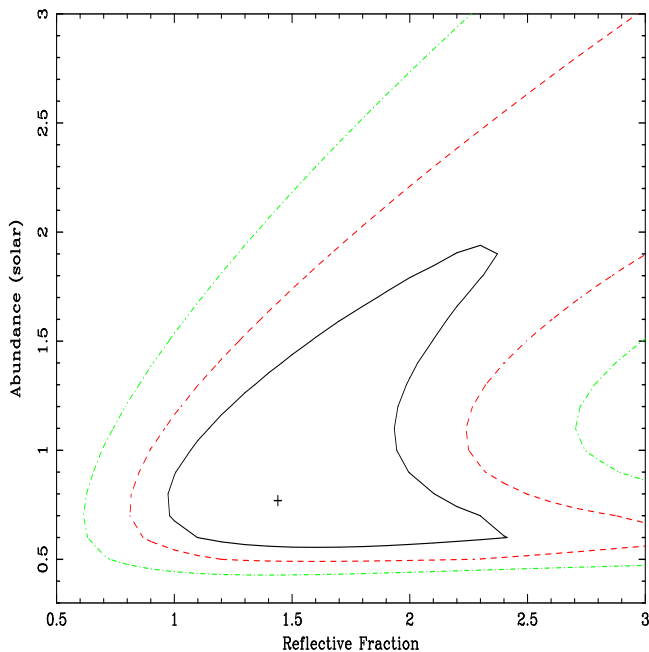


Figure 6. Confidence contours (corresponding to 68 per cent, 90 per cent, and 95 per cent confidence levels) for abundance vs. reflective fraction relationship for fits in the energy range $4 \text{ keV} < E < 20 \text{ keV}$.

4 TEMPORAL AND SPECTRAL CHANGES

Having convinced ourselves that reflection is needed to model our data, we next investigate the effects of temporal changes in the light curve on spectral components. To do this, we divide our light curves into three groups based on the countrate. Accordingly, we define i1, i2, and i3 to be respectively the intervals with average count rates ~ 14 , 9, and 20 counts per second. Figure 1 shows that this also corresponds roughly to the time intervals 0–3 ks, 100–200 ks, and 200–300 ks.

We have searched for spectral changes between the different periods of data. From our theoretical pre-conceptions, we also wish to address whether any changes we see are due to an intrinsic change in the power law slope, the reflection continuum changing, or a combination of both.

Initially, we take a simple approach and fit a simple power law plus gaussian component in the 4–10 keV energy range, and a simple power law to the 10–20 keV range. The 4–10 keV range should be relatively unaffected by the reflection component, whereas the 10–20 keV range is very much affected by reflection. These fits are presented in Table 1. It can be seen that there is evidence for spectral variability between these different flux states. In particular, the 4–10 keV photon index is significantly steeper in the brightest period. In addition, there may be some evidence for a relative flattening of the 10–20 keV range in the lowest flux state implying a possible increase in reflective fraction (this agrees with the more complicated fit that includes the reflected spectrum shown in Table 2), although the errors are too large to make definitive statements. The increase of the iron line strength in this low period would support such a hypothesis.

We next use the PEXRAV model to investigate more rigorously the relationship between the spectral components, Γ and the reflective fraction. This is an important issue to address since it has direct bearing on the physics of the central engine. For example, if the spectral variability can be shown to originate purely from a change

CHANGE IN Γ FOR DIFFERENT STATES OF MCG–6-30-15

Interval	Γ_{4-10}^a	Γ_{10-20}^b	W^c (eV)	Flux ^d
i1	$1.89^{+0.1}_{-0.11}$	$1.53^{+0.32}_{-0.36}$	327^{+112}_{-80}	4.06
i2	$1.86^{+0.09}_{-0.1}$	$1.29^{+0.22}_{-0.35}$	446^{+85}_{-82}	2.51
i3	$2.10^{+0.05}_{-0.04}$	$1.69^{+0.13}_{-0.12}$	253^{+35}_{-48}	6.03

Table 1. Results are quoted from simple power law fits. ^a Power-law photon index in for $4 \text{ keV} < E < 10 \text{ keV}$. ^b Power-law photon index for $10 \text{ keV} < E < 20 \text{ keV}$. ^c Equivalent width of the iron emission line. ^d 2–10 keV flux in units of $10^{-11} \text{ erg cm}^{-2} \text{ s}^{-1}$

in the photon index of the primary source (with constant reflective fraction), changes in the conditions of the X-ray emitting disk-corona would then be strongly implicated. On the other hand, the different temporal states may be due to the amount of reprocessing in the source; for example, the gravitational bending/focusing as the X-ray source gets closer to the black hole will enhance the amount of reflection (e.g., Martocchia & Matt 1996). Fig. 7 shows the confidence contours on the reflective-fraction/photon-index plane for these three periods of data. To improve our constraints, the abundances of the reflector have been fixed at the best-fit value found from the total dataset ($Z = 0.77Z_{\odot}$; Section 3.2). We are justified in fixing these abundance since, on physical grounds, we do not expect them to vary between our three intervals. Given that we have fixed the elemental abundances, we also fixed the ratio between the iron line equivalent width and the reflective fraction such that a reflective fraction of unity corresponds to an iron line equivalent width of 150 eV (appropriate for the above choice of abundances; see Reynolds, Fabian & Inoue 1995).

As suspected on the basis of the simple power-law fits in Table 1, Fig. 7 (using a more complicated fit that includes the reflected spectrum) shows that the steepening in primary photon index during the brightest period of data is statistically significant. There is also a suggestion of an increase in reflective fraction (with constant Γ) when going from the intermediate flux state to the low flux state. Thus it appears that both changes in the properties of the primary X-ray source and changes in the amount of reflection are relevant for understanding spectral variability. As a further check on the robustness of these results, we have recreated contours similar to those in Fig. 7 for several choices of abundances within the 68 per cent confidence statistical error range, and find that none of the results changes materially based on these choices of abundance values. The discrepancy in Γ between i3 and the other two states does diminish if the abundance is allowed to be a free parameter. It should be noted that the model as currently implemented does not include relativistic blurring of the reflection component. A major caveat to RXTE spectral variability results lies in the background models.

5 DISCUSSION

The purpose of this paper was to show what unanswered questions can be addressed with the large area and wide-band coverage of RXTE even with the current uncertainties in spectral calibration. The presence of a broad iron line is clearly evident as shown with a simple power law fit, and is one of the first detections where both features are seen simultaneously. We add a reflection component to our power law and gaussian fit to find that reflection is necessary to describe our data. We note also that the steep intrinsic photon index

SPECTRAL FITS USING POWER-LAW WITH REFLECTION MODEL FOR DIFFERENT STATES OF MCG-6-30-15								
Data	Γ_{4-20}^a	A^b	reff ^c	LineE ^d	$I_{K\alpha}^e$	W^f (eV)	Flux ^g	χ^2
i1	$2.01^{+0.25}_{-0.19}$	$1.61^{+0.58}_{-0.39}$	$1.55^{+2.29}_{-2.03}$	$5.99^{+0.23}_{-0.21}$	$1.44^{+0.45}_{-0.64}$	283^{+88}_{-126}	6.83	21
i2	$2.04^{+0.22}_{-0.18}$	$1.01^{+0.34}_{-0.22}$	$1.95^{+2.36}_{-1.08}$	$6.17^{+0.15}_{-0.14}$	$1.11^{+0.23}_{-0.34}$	374^{+77}_{-115}	4.26	23
i3	$2.22^{+0.08}_{-0.08}$	$3.45^{+0.44}_{-0.37}$	$1.28^{+0.56}_{-0.42}$	$6.15^{+0.08}_{-0.13}$	$1.26^{+0.34}_{-0.27}$	182^{+49}_{-39}	9.12	32

Table 2. ^a Power-law photon index. ^b Power-law flux at 1 keV, in units of 10^{-3} ph cm² s⁻¹ keV⁻¹. ^c Reflective fraction = $\Omega/2\pi$. ^d Energy of the iron $K\alpha$ emission line. ^e Intensity of iron emission line in units of 10^{-4} ph cm⁻² s⁻¹. ^f Equivalent width of the emission line. ^g 2-20 keV flux in units of 10^{-11} erg cm⁻² s⁻¹. ^h χ^2 for 36 degrees of freedom

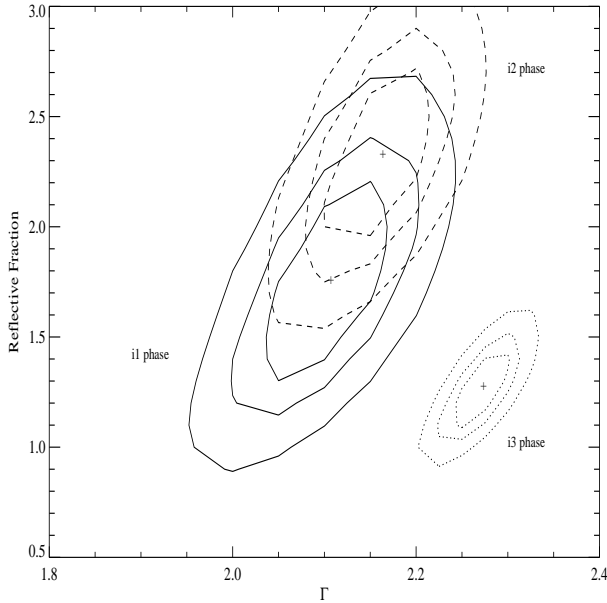


Figure 7. Confidence contours (corresponding to 68 per cent, 90 per cent, and 95 per cent confidence levels) showing the relationship between Γ and reflective fraction for i1, i2, and i3 phases of MCG-6-30-15 light curve during the period from 1996 September 15 to 1996 September 25.

coupled with a narrow $H\beta$ FWHM implies that MCG-6-30-15 can be a possible narrow-line Seyfert 1 galaxy candidate.

While spectral results may change in detail over the course of the next year with further improvements in calibration, we can already begin to place upper bound limits on the relationship between abundance values and reflective fraction.

In Section 4, we study the effects of temporal variability on spectral components and find evidence to support the notion that variability may be due to changes in the amount of reflection seen (e.g. due to gravitational or Doppler beaming of the primary emission towards the disk). It is however not clear whether this effect may also be coupled with contributions from changes in the properties of the source itself (e.g. the temperature and optical depth of the coronal plasma). We expect to be able to resolve these issues better with longer looks and simultaneous ASCA observations. For the time being, the present results are important observational first steps in understanding some of the physics of AGN reprocessing mechanisms, and push the limits of our knowledge.

6 ACKNOWLEDGEMENTS

We thank all the members of the RXTE GOF for answering our inquiries in such a timely manner, with special thanks to Keith Jahoda for explanations of calibration issues. JCL thanks the Isaac Newton Trust, the Overseas Research Studentship programme (ORS) and the Cambridge Commonwealth Trust for support. ACF thanks the Royal Society for support. CSR thanks the National Science Foundation for support under grant AST9529175, and NASA for support under the Long Term Space Astrophysics grant NASA-NAG-6337. KI and WNB thank PPARC and NASA RXTE grant NAG5-6852 for support respectively.

REFERENCES

- Boller Th., Brandt W. N., Fink H., 1996, *A&A*, 305, 53
 Brandt W. N., Mathur S., Elvis M., 1997, *MNRAS*, 285, L25
 Fabian A. C., et al, 1994a, *PASJ*, 46, L59
 George I. M., Fabian A. C., 1991, *MNRAS*, 249, 352
 Guilbert P. W., Rees M. J., 1988, *MNRAS*, 233, 475
 Iwasawa K., Fabian A. C., Reynolds C. S., Nandra K., Otani C., Inoue H., Hayashida K., Brandt W. N., Dotani T., Kunieda H., Matsuoka M., Tanaka Y., 1997, *MNRAS*, 282, 1038
 Lightman A. P., White T. R., 1988, *ApJ*, 335, 57
 Magdziarz P., Zdziarski A., 1995, *MNRAS*, 273, 837
 Martocchia, A., Matt, G., 1996, *MNRAS*, 282, L53
 Matsuoka M., Yamauchi M., Piro L., Murakami T., 1990, *ApJ*, 361, 440
 Nandra K., Pounds K. A., 1994, *MNRAS*, 268, 405
 Nandra K., Pounds K., Stewart G. C., 1990, *MNRAS*, 242, 660
 Nandra K., Pounds K., Stewart G. C., Fabian A. C., Rees M. J., 1989, *MNRAS* 236, 39p
 Otani C., Kii T., Reynolds C. S., Fabian A. C., Iwasawa K., Hayashida K., Inoue H., Kunieda H., Makino F., Matsuoka M., Tanaka Y., *PASJ*, 48, 211
 Pounds K. A., Nandra K., Stewart G. C., George I. M., Fabian A. C., 1990, *Nat.* 344, 132
 Reynolds C. S., 1996, *PhD thesis*
 Reynolds C. S., Fabian, A. C., 1997, *MNRAS*, 290, L1
 Reynolds C. S., Fabian A. C., Inoue H., 1995, *MNRAS*, 276, 1311
 Reynolds C. S., Fabian A. C., Nandra K., Inoue H., Kunieda H., Iwasawa K., 1995, *MNRAS*, 277, 901
 Reynolds C. S., Ward M. J., Fabian A. C., Celotti A., 1997, *MNRAS*, 291, 403
 Rees M.J., 1984, *A&AR*, 22, 471
 Tanaka Y., Nandra k., Fabian A. C., Inoue H., Otani C., Dotani T., Hayashida K., Iwasawa K., Kii T., Kunieda H., Makino F., Matsuoka M., 1995, *Nat.*, 375, 659